Evaluation of an underwater laser scanner and an air-borne laser scanner in coastal shallow waters

Annette Scheider [1], Sethmiya Herath Mudiyanselage [1], Christoph Werner [2], Ellen Heffner [1], Annika L. Walter [1], Jannis Gangelhoff [2], Harald Sternberg [1]

[1] HafenCity University Hamburg, Hamburg, Germany – (annette.scheider, sethmiya.mudiyanselage, ellen.heffner, annika.walter, harald.sternberg)@hcu-hamburg.de
[2] Fraunhofer Institute for Physical Measurement Techniques IPM, Freiburg, Germany – (christoph.werner, jannis.gangelhoff)@ipm.fraunhofer.de

Keywords: Underwater LiDAR, Bathymetric LiDAR, Hydrography, Point Cloud Quality

Abstract

Next to the known photogrammetric or acoustic measurement techniques, nowadays LiDAR is a promising option for high-resolution surveys or monitoring of underwater structures in low turbid and shallow waters. The objective of this investigation is to determine the performance of an underwater laser scanner and an air-borne bathymetric laser scanner for mobile data acquisitions. For this purpose, the underwater LiDAR (ULi) from Fraunhofer IPM is installed on a vessel. To enable the registration and georeferencing of the scan data, ULi is added by an Inertial Navigation System (INS) and two GNSS antennas. On the other hand, the air-borne bathymetric laser scanner (ABS) is integrated into an unmanned aerial system (UAS). Both systems are used to survey in the same measurement area to acquire comparable data sets. With the selected measurement settings, both systems can penetrate through water for more than 10 m and are able to resolve small underwater structures. Caused by shorter measurement ranges, ULi offers a point density which is approximately four times higher than the ABS and is able to resolve vertical underwater structures. The advantage of the UAS mounted ABS is that it can survey in shallow areas which cannot be accessed by vessels.

1. Introduction

High-resolution and high-precision surveys or monitoring of fine-scale underwater structures is still challenging, especially if a 3D point cloud is required. Modern acoustic instruments, multibeam echo sounders (MBES), can achieve an accuracy from a to few centimetres up to 1 dm in shallow waters. For detailed object acquisition, MBES with measurement frequencies of 300 kHz – 700 kHz are used. However, even if certain MBES with deeper measurement frequencies can cover measurement ranges of several kilometres, measurement frequencies of 700 kHz can normally only be used for much shorter measurement ranges. Kongsberg (2022) indicates a typical range of 45 m for the Kongsberg EM 2040P MKII in cold ocean water. However, the resolution is limited by the wavelength of the acoustic signal. For underwater close-range applications, there is also a potential to use optical systems. Generally, the measurement range of optical acquisition methods is limited by turbidity, varying refraction coefficients and the absorbing characteristics of water. Thus, they can only be used for close range under water applications. Balletti et al. (2015), Burns et al. (2015), Lochhead and Hedley (2022) and others have shown, that underwater photogrammetry can achieve high quality in clear water if the light conditions are favourable and adequate enhancement methods are applied. Structure from Motion (SfM) can be used to calculate 3D point clouds.

Besides, laser scanners for underwater applications have been developed. Airborne based bathymetric LiDAR were developed in the 1960s (Guenther, 1995). The emergence of efficient unmanned aerial systems (UAS) enables area-wide surveying with these instruments. This development is supplemented by purely underwater laser scanners. These scanners are already used on Remotely Operating Vehicles (ROV) and Autonomous Underwater Vehicles (AUV) for several years (Bleier et al., 2019, Castillón et al., 2019). In recent years, underwater laser scanners with mechanical beam steering by rotating prisms have been further developed. For instance, Fraunhofer IPM has developed an Underwater LiDAR instrument (ULi) whose scan pattern can be adapted by the user as well as an air-borne bathymetric scanner (ABS) (Werner et al., 2023). Both systems, the underwater laser scanner and the air-borne laser scanner are used for mobile data acquisition. In this context, they are investigated in a real-world environment in shallow seas with clear water conditions. The presented study intends to verify the performance of the ULi and the ABS in comparison.

2. Concept of the investigation

For the real-world scenario, the instruments will be used in or respectively above the sea in very shallow waters. It will be investigated which performance and quality can be achieved for mobile data acquisition and if the acquired 3D data of the sea ground can supplement each other in mapping very shallow waters.

2.1 Objectives

While the ABS has already been used for mobile mapping application (Werner et al., 2023), ULi was mostly used in static underwater set-ups (Heffner et al., 2025a, Heffner et al., 2025b, Lan et al., 2025). This investigation focuses on its installation for a mobile data acquisition. For this purpose, a workflow is presented starting with installation, calibration and data processing. In order to investigate the performance of the ULi and the ABS in shallow sea environments, different criteria are considered to evaluate the quality of the point cloud. The geometric quality of the point cloud depends highly on the performance of the navigation solution. Therefore, its estimated accuracy is considered. The penetration depth or respectively measurement range expresses the maximum distance between an underwater object and the scanner (ULi) or respectively the water surface (ABS). In order to express the completeness, its radial, along-track and across track resolutions, and the point density are determined. Here, the point density P, the number of neighbouring points, is calculated within a radius of 1 m. The completeness of object acquisition or respectively coverage of the point cloud is also calculated. For this purpose, selected point cloud sections are represented by a best-fit plane and its normal vector $\boldsymbol{n}$. Each plane is used to establish a local coordinate system (x_l, y_l, z_l) whose vertical axis (z_l) is parallel to the *z*-axis of the point cloud coordinate system. The x_l, y_l axes are aligned in a plane which is parallel to the horizontal plane of the point cloud system, and one of them is aligned along the horizontal component of $\boldsymbol{n}$. In the next step, the rotated point cloud is projected onto a horizontal plane and a vertical plane, similar to Rebolj et al. (2017). Each projection plane is rasterized into square cells. To ensure a representative cell size, its definition depends to the determined along-track resolution of the point cloud. In each case, the omission rate OmR quantifies the number of empty cells (k_o) with respect to the complete number of cells (k) covering the complex hull of the respective point cloud section,

$$OmR = \frac{k_o}{k}. \tag{1}$$

The structure of the sea ground can be expressed by the distance between a local best-fit plane and an individual point. CloudCompare (2022) describes it as parameter *roughness*. By using small best-fit planes, whose size depends to the resolution of the point cloud, this approach can also be used to express the noise level of the point cloud. Here, this parameter is labelled *noise distance* (*nd*) in order to distinguish it from parameter *roughness*. The roughness *(rough)* is calculated for best-fit planes with a radius of 1 m.

2.2 Measurement site

The measurement site is in the Seribu National Park, Indonesia, close to Pulau Pramuka and Pulau Panggang. The ULi and the ABS are operated in waters with a Secchi depth of 10 m – 13 m. The seafloor in this area consists of flat, likely sandy areas, reefs, and of natural (e.g., rocks, sea grass, corals) and artificial objects (e.g., tyres, piles). The measurement campaign took place in September 2025. The World Ocean atlas (NOAA, 2023) indicates an average salinity of 33 % - 34 % and a water temperature of ca. 30 °C for this month. According to Höhle (1971), this causes a refraction index of approximately 1.342.

Figure 1: Very shallow water area with a seagrass field and a water depth of ca. 1 m

The measurement site caused certain challenges for the survey campaign. Since the islands are surrounded by very shallow areas and reefs with water depth of less than 2 m, usually ships cannot approach these parts of the coast. These areas could only be surveyed by the UAS-integrated ABS. An example for such an area is the seagrass field in Figure 1. Nevertheless, the range and batteries of the UAS are limited, so the reefs and objects behind a distance of approx. 500 m away from the islands could only be mapped with ULi. Certain parts of the measurement site could be surveyed by both systems. While the UAS could fly along the planned survey lines, it was not possible to follow planned lines with the ship and ULi due to external circumstances and incompletely mapped shallow waters.

3. Instruments and Measurement configuration

Both instruments, the ULi and the ABS, are installed on mobile platforms for mobile data acquisition. While the ABS is installed on a remotely controlled platform (UAS), ULi is mounted on a small vessel. In both cases, the installation set up is adapted to their individual characteristics.

3.1 Underwater LiDAR system (ULi)

The underwater laser scanner ULi (Figure 2a) emits a rotating laser beam, which is controlled by a rotating double wedge prism (Werner et al., 2023). The scan pattern can be adjusted within a field of view of 44° (IPM, 2026). Here, the laser beam rotates with a constant tilt of the rotation axis, so the resulting scan pattern is a spiral. The ULi uses a laser wavelength of 532 nm and the Time-of-Flight (ToF) principle to determine the distance between scanner and object (Werner et al., 2023). It has a sampling frequency of up to 100,000 points per second. To optimize the data acquisition in different environments, the energy of the emitted laser beam can be adapted. There are two laser operation modes which can be selected according to the water turbidity and the material of the scanned object: the unfiltered laser mode which is classified as a 3B laser and a filtered adjustment mode with laser class 2M (according to EN 60825-1:2014). Heffner et al. (2025) describe a maximum measurement range in the unfiltered mode of 17 m in low turbid fresh water (0.9 NTU), while the range is reduced to 1.4 m in turbid water (4.5 NTU). In each case, the lateral resolution is better than 2.95 mm for a stable scanner position (Heffner et al., 2025). Heffner et al. (2025) also determine the size of underwater objects and derives a relative range accuracy of -3.37 mm for 1 cm object distance. Walter et al. (2025) investigate the performance of the scanner for different object materials and describe that bright, reflective materials reduce the measurement noise compared to dark, matt materials. Similar to terrestrial laser scanners, the scattering of the point clouds increases with the roughness of the object surface. This investigation confirms the results of Chen et al. (2020).

(a) (b)

Figure 2: (a) ULi (Fraunhofer IPM) with attached INS housing, (b) pole-mounted installation of ULi

For mobile applications, ULi is installed on a vessel and it is mounted on a pole (Figure 2b). Therefore, additional sensors have to be added to enable the determination of a georeferenced point cloud. For this project, ULi is equipped with an Inertial Navigation System (INS, Figure 2a), a SBG Quanta Micro with a MEMS inertial measurement unit, which is connected to two multi-frequency GNSS antennas. The INS itself is in a waterproof case and is firmly attached to the backend of ULi’s cylindrical housing. SBG (2025a) states a roll and pitch accuracy of 0.01° and a heading accuracy of 0.035° in post-processing mode. This enables flexible trajectory determination and the ULi does not have to be connected to another motion sensor onboard. To be able to survey vertically aligned structures (e.g. quay structure), the sea ground but also natural reefs or ridges, an inclined installation of the laser scanner is beneficial. The scanner is mounted with an inclination of 30° with respect to the horizontal plane and it is roughly orientated to the ship’s transverse direction. Table 1 shows for simulated measurements that this configuration allows the acquisition of different types of underwater environments.

Table 1: Simulated amount of points in a 1 m wide cross section on a plane (vertical or resp horizontal distance: 10 m) for the applied measurement settings within an assumed measurement range of 13 m; installation angle with respect to the horizontal plane

Installation angle of ULi	0°	30°	60°	90°
Flat ground	0	3,211	15,519	24,276
Slope (45°)	10,368	24,339	24,337	10,368
Vertical wall	12,136	15,526	3,215	0

3.2 Air-borne Bathymetric Laser Scanner

The ABS, a topobathymetric LiDAR system, uses two wavelengths: a green laser with a wavelength of 532 nm and a 1,064 nm infrared laser (Werner et al., 2023). While the green laser penetrates the sea surface, the infrared pulse reflects off the sea surface (Mandlburger and Pfennigbauer, 2011). The used system applies a Nd: YAG laser. The system operates with a nominal pulse repetition rate of 35 kHz for short range applications and was adopted for 1-2 Secchi depths (IPM, 2025). Rather than limiting each transmitted laser pulse to a single detected return, modern systems take advantage of high-speed field-programmable gate arrays (FPGAs) to record the entire backscattered signal at high temporal resolution (Mandlburger and Pfennigbauer, 2011). This approach, commonly referred to as full-waveform processing, provides valuable information about the vertical structure and density of underwater vegetation and improves the interpretation of complex aquatic environments.

Figure 3: ABS (Fraunhofer IPM) mounted on a UAV

The ABS has a weight of 2.5 kg without batteries. For mobile measurements, it is firmly attached to an UAS (Figure 3). The laser scanner features an elliptical scan pattern with a maximum inclination of 15° off-nadir (Werner et al., 2023). For positioning and attitude determination, this mobile system is equipped with a GNSS-antenna and the same INS as the ULi.

3.3 Calibration

Next to a variety of internal parameters, the offsets and boresight angles between the IMU and the GNSS-antenna(s) within the platform coordinate system have to be determined. Since the set-up of the ABS on a UAS does only slightly change between subsequent flight-campaigns, it is assumed that the installation of ULi is more prone to deviations in the installation parameters. On one hand, this can be attributed to the pole-mounted installation which is influenced by the relative water current and the stability of the installation. On the other hand, ULi can be installed on different vessels. Subsequently, the installation parameters have to be newly determined in a system calibration (field calibration). In hydrography, offsets are often determined with a total station or a laser tracker on a shipyard. This concept allows to determine offsets with an accuracy of a few millimetres (Brüggemann, 2013). Meanwhile, boresight angles and synchronization parameters are often determined by a field calibration, e. g. the Patch test (IHO, 2011) or the MIBAC test (Seube and Keyetieu, 2017). Here another approach is applied for both systems: It requires to fly or drive multiple curves, e.g. eight-shaped curves (SBG, 2025b) which cause a significant change of attitude. The lever arms between the INS and GNSS antenna(s) are roughly determined before. The software Qinertia/SBG Systems can estimate and improve the offsets (lever arms) and the boresight angles by considering them as state variables within the applied Extended Kalman Filter (SBG, 2025b).

The alignment of the internal scanner coordinate system with respect to the INS coordinate system is determined in a system calibration before the survey campaign.

3.4 Processing

The measurement data is stored in the instruments themselves and can be transferred after the measurements. The data recorded on the mobile platforms have to be post-processed. Firstly, the navigation data is processed with the software Qinertia by applying a forward-backward filter.

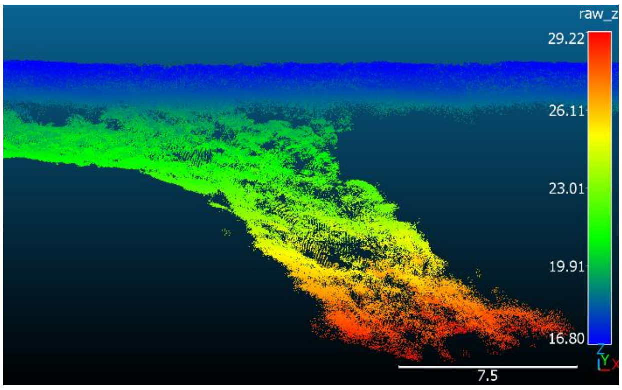

Figure 4: Section of the ABS point cloud including an underwater slope at a reef edge, visualization with CloudCompare (2024), colorized by vertical distance

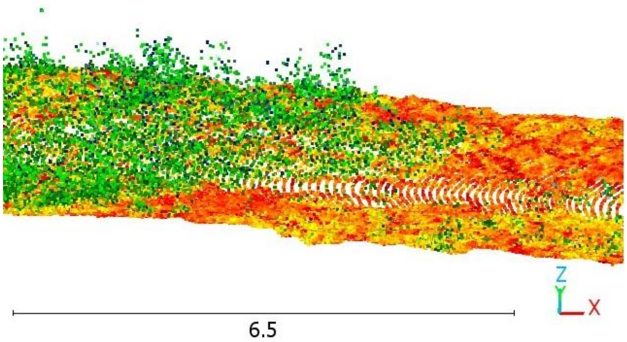

Figure 5: Details of the ABS point cloud: Seagrass field (green) and sandy ground (orange/red), visualization with CloudCompare (2024), colorized by intensity

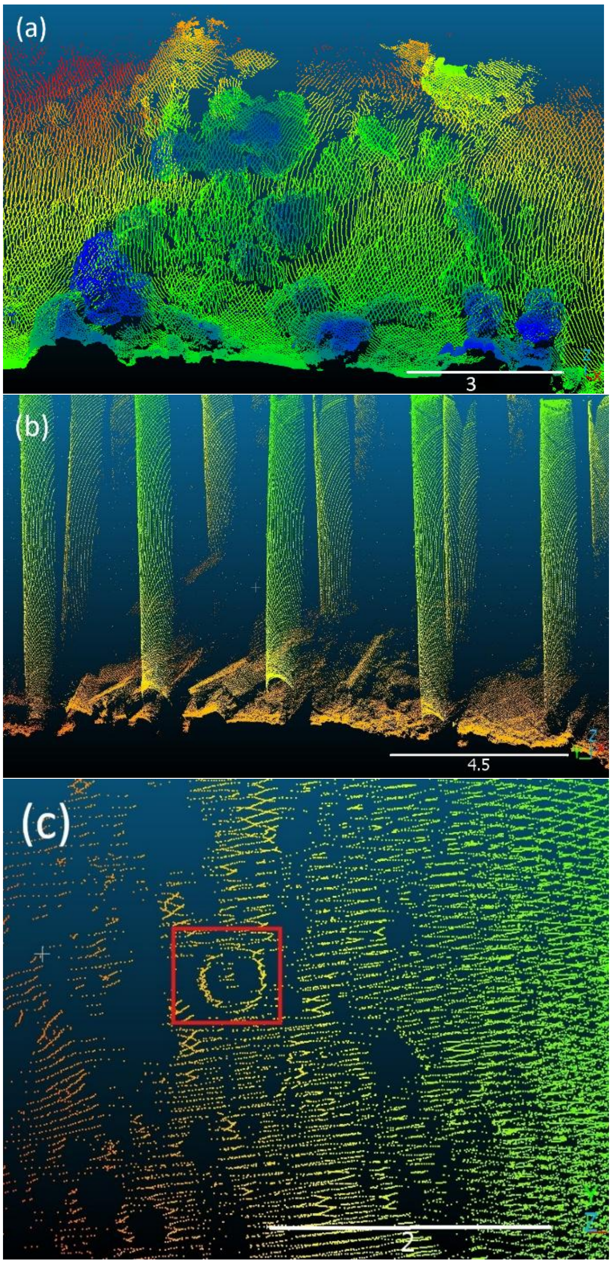

Figure 6: Processed mobile ULi data – point cloud with (a) sloped ground with rocks, (b) piles as a quay foundation and (c) small structures like a tyre – visualization with CloudCompare (2024), colorized by distance

For a precise navigation solution, a control point on Pramuka island is used to set up the GNSS base station. It provides further GNSS observations to determine a precise differential GNSS solution. The required offsets and installation angles are estimated and improved within this step.

The navigation solution and the stored LiDAR data are imported in the proprietary Software Pulsalyzer to process and georeference the scan data. For that purpose, the correct refraction index has to be selected. Even though both instruments are designed to acquire full waveform signals, only the strongest pulse reflection of each signal are detected during the performed first data processing.

The resulting point cloud is exported in the *.las format for further analysis. The processed point cloud of the ULi indicates small natural and artificial objects on the sea ground (Figure 6a and c) and vertically aligned infrastructure objects (Figure 6b). Also, the ABS data contain details of rocks on a underwater slope (Figure 4). Another ABS point cloud shows the appearance of a seagrass field (Figure 5) which is also depicted in Figure 1.

4. Analysis

The surveys of ABS and the ULi were not operated parallelly in the same measurements site. The analysed ABS data were acquired on 21 and 23/09/25 while the presented surveys with the ULi were performed on 23 and 24/09/25. For this reason, the external condition (e.g., water turbidity, atmospheric parameters) for the measurements are slightly different.

4.1 Navigation solution

The GNSS observations are processed as a precise differential GNSS-solution by using observations of a GNSS base station. The baseline has a length of maximum ca. 1.1 km. The accuracy of the post-processed navigation solution for the individual survey lines highly depends on the quality of the acquired GNSS data and also to the stability of the determined calibration parameters. The considered accuracies are calculated with the software Qinertia. The quality of the GNSS data for this campaign was not ideal. It was not possible to achieve a fixed GNSS solution for certain parts of the trajectory. The UAS flights were conducted with a velocity of ca. 5 m/s and a flight height of 20 m above the sea surface while the ship was moving with a velocity of ca. 1 – 2 m/s. Due to the current and the manoeuvres, the vessel velocity varies within each survey line.

Table 2: Standard deviations (Stdv) of the post-processed, filtered position and attitude

Stdv. - component	**Vessel (ULi)**	**UAS (ABS)**
σ – East [m]	$\leq$ 0.017	$\leq$ 0.013
σ – North [m]	$\leq$ 0.013	$\leq$ 0.010
σ – Height [m]	$\leq$ 0.027	$\leq$ 0.014
σ – Roll [°]	$\leq$ 0.009	$\leq$ 0.007
σ – Pitch [°]	$\leq$ 0.007	$\leq$ 0.006
σ – Heading [°]	$\leq$ 0.027	$\leq$ 0.070

According to Table 2, the standard deviations σ of the UAS coordinates are smaller than those of ULi. The difference in the East and North coordinate component is 3 mm or respectively 4 mm. Even if it has to be mentioned that the standard deviation of the UAS is increased to 1.7 cm for a short time interval, its heights is up to 1 cm more accurate compared to the vessel’s heights. The standard deviations of the roll and pitch angles are also slightly more accurate for the UAS. These results benefit from the dynamic trajectory. In contrast, the heading solution for the vessel is ca. factor 2.6 more accurate compared to the UAS results. This is because two GNSS antennas are installed on the vessel. Their base length of ca. 3.2 m contributes to a more accurate heading solution while the UAS is only equipped with one GNSS antenna.

There are different reasons for the lower positioning accuracy of the vessel: On the one hand, there were multiple outages of the GNSS base station on 24/09/2025. But on the other side, it is assumed, that there was a deformation of the installation framing on the ship itself. This resulted in deviations of the installation parameters compared to the parameters determined in the calibration.

4.2 ULi point cloud

On 24.09.2025, the determined Secchi depth varied between 10 m to 12 m in the direct vicinity of the measurement areas. However, local variations might have occurred. Depending on the selected filter of the transmitted laser, the achievable measurement range differs. As Figure 7 shows, the range in the direction of the longitudinal axis of the laser scanner in the unfiltered laser mode (none) varies between ca. 10.17 m and 14.3 m, while the filtered laser mode (medium) results in ranges between ca. 8.55 m and 10.08 m. Mounted close to the water surface, ULi achieves a penetration range of approx. 1.16 $*$ Secchi depths for this inclined installation. The maximum longitudinal ranges result in measured 3D distances (scanner – distinct surveyed points on an object) of up to 15.76 m. It has to be remarked, that the results in Figure 7 highly depend to the distribution of the objects within the measurement area.

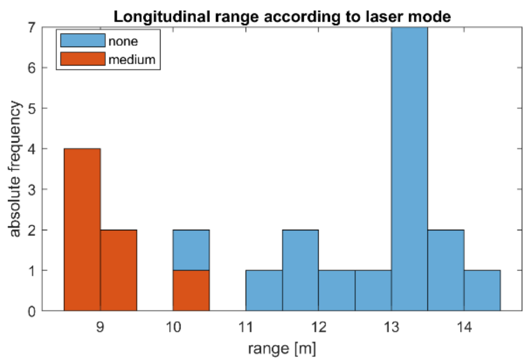

Figure 7: Maximum range in longitudinal scanner direction for the filtered (medium) and in the unfiltered (none) laser mode (24.9.2025)

The radial resolution is provided with a sub-millimetre resolution. The considered measurements were carried out either by surveying artificial structures or a reef consisting of a rocky slope. The resolution between two consecutive points in the point clouds is mainly influenced by the laser rotation frequency and measurement distance. In the considered datasets, the mean distance between two consecutive points in regularly scanned sections is approx. 1.4 cm. Besides, the along-track resolution (distance between two consecutive laser rotations) of the point cloud depends highly to the vessel's velocity. For the considered datasets the resolution is determined exemplarily in distance ranges of approx. 10 m and ranges from ca. 7.6 cm of up to 9.9 cm. This allows the detection of small objects like it is depicted in Figure 6c. The object has an estimated diameter of ca. 46 cm and a height of approx. 6 cm above ground. It is assumed to be a tyre. The radii of 15 randomly selected piles depicted in Figure 6b are also estimated. For that purpose, best-fit circles are estimated in a cross section of the point cloud with CloudCompare (2024). The mean radius is 0.409 m, with an empirical standard deviation of 3.9 cm.

The point density P of the point cloud is calculated in CloudCompare (2024). For that purpose, three point cloud sections are considered. The results in Table 3 emphasize that section #2 having the closest distance to the scanner has the highest point density and also the lowest roughness. The large difference between max(P) and median(P) in section #3 is caused by changing roughness. This section partly includes some rocks.

Table 3: Section characteristics and point densities [Points/m²] in the ULi point cloud for the individual sections

Section	**#1**	**#2**	**#3**
Max(*rough*)	61 cm	51 cm	64 cm
Mean(*nd*)	1,3 cm	1,3 cm	1,2 cm
Inclination	37,71°	39,21°	39,80°
Point density P			
Mean (P)	12,507	11,897	10,514
Median (P)	13,467	11,452	10,866
Max (P)	22,783	25,431	21,599
Min (P)	1	1	13

The scattering of the points in the three section is approx. 1.3 cm (Table 3) with respect to the surrounding points. Considering the accuracy of the navigation solution, this is an acceptable result. The respective noise distances for the complete survey line's point cloud are always lower than 8.7 cm.

4.3 ABS point cloud

Caused by the shallow water area, the ABS cannot use its full penetration depth potential. For a flight height of approx. 20 m above the water surface, its laser beam could penetrate 12,28 m into the water with the chosen scan settings. In this case, the across track resolution is approx. 3.9 cm in a water depth of ca. 3 m. The along-track resolution is approx. 11 cm.

However, the ABS point cloud contains a higher degree of measurement noise. Considering the bathymetry, the noise distance is ca. 3 cm. The roughness of the sea ground in the point cloud is up to 52 cm in a steep and deeper water zone (section #A2) which is depicted in Figure 5a. This roughness value (Table 4) is partly originated by the inhomogeneous, rocky structure of the sea ground. But it is obscured by scattering in the water column. In flat and very shallow water zones (section #A1 with ca. 2.5 m water depth) the maximum roughness is ca. 31 cm for some objects which are assumed to be stones. Nevertheless, the height of the seagrass field in the point cloud (Figure 5) above ground is determined to be ca. 1 m which approximately coincides with the real situation. Table 4 also presents different point densities in the two sections: The mean and the median point densities in section #A1 are 1.9 or resp. 2 times higher than in section #A2. For the complete data set (including #A1 and #A2), mean(P) is 2883.

Table 4: Point densities [Points/m²] in one line of the ABS point cloud for the individual sections and section characteristics

Section	**#A1**	**#A2**
Max(*rough*)	31 cm	52 cm
Mean(*nd*)	3 cm	3 cm
Inclination	2,62°	38,05°
Point density P		
Mean (P)	3014	1622
Median (P)	2767	1416
Max (P)	5838	4871
Min (P)	836	5

https://doi.org/10.5194/isprs-archives-XLIX-B2-2026-989-2026

4.4 Potential for a combined survey

Neither of the investigated surveying systems can achieve a perfect 3D coverage of the point cloud on a rough sea ground. Depending to the instrument's mounting, the acquired parts of the sea ground differ. To emphasize this aspect, the omission rates OmR within a convex hull around the projected point cloud is determined. The parameter h_OmR indicates the OmR for a projection onto a horizontal plane and v_OmR for a vertical plane. The considered cell size is 10 cm x 10 cm. As expected, Table 5 shows that the ABS achieves a very low h_OmR of less than 0.04 which indicates a very high coverage in the horizontal component. The v_OmR values are higher and range from 0.212 to 0.269. The v_OmR values for the ULi point cloud are similar. But these values are strongly influenced by the structure of the sea bed. Especially the sections #1 and #3 have a rougher structure of the sea ground (

Table 4) compared to the sections #A1 and #A2. The vertical structures tower other elements inside the section. Therewith, they enlarge the area of the projected point cloud. This issue partly influences the number of empty cells within the considered convex hull and the seemingly high omission rates.

Table 5: Omission rates of the projected point clouds

Section	h_OmR	v_OmR
ULi		
#1	0.173	0.195
#2	0.250	0.212
#3	0.228	0.244
ABS		
#A1	0.027	0.269
#A2	0.0353	0.212

5. Conclusion

This investigation shows first results for a mobile data acquisition with the ULi. The resulting point cloud is extended to very shallow waters (water depth < 2 m) by ABS operations. Both instruments provide good results in the shallow tropical sea. At a Secchi depth of 10 m to 12 m and a salinity of ca. 34 %, the underwater measurement range of the ULi is up to 13.7 m in sea water while the ABS can penetrate ca. 12.3 m into the water. The results highly depend to the applied driving or flying speed, to the specified scan settings, the environmental parameters and to the geometric quality of the navigation solution. The applied settings and speed the detection of objects with a size of a few centimetres in beam direction and in the direction of the tangent. In normal direction, the objects should cover an area of a few decimetres. This value might be improved by reducing the speed of the mobile platform. The improvement of the accuracy of the navigation solutions, especially the GNSS solution, offers further potential for more accurate point clouds. However, the water temperature and salinity must be known.

Caused by the different installation direction of the ULi and the ABS, the coverage of the data sets differ. The ULi can scan vertical underwater structure while the ABS only scans the top side of these structures. However, its installation on a UAS allows the data acquisition of wider area stripes compared to ULi and it can access very shallow waters which are not approachable for most of the ships. For this reason, the two instruments complement each other well for applications in this measurement site. Generally, the UAS mounted ABS can be used to cover a large area quickly and efficiently. Based on this data, the ULi mounted on a ship or oven on an autonomous or remotely operated vehicle is able to survey or monitor certain objects in close range with a high resolution.
Future work will focus on data collection using ABS, ULi, multibeam echo sounders, and a hyperspectral camera in the same area for combined analysis. The integration of a hyperspectral camera will be helpful for the advanced analysis and validation of the features detected from the ABS and ULi. Furthermore, upcoming research will explore the application of advanced machine learning and deep learning approaches for automatic feature detection and classification using ULi and ABS data.

6. Acknowledgment

The measurements were acquired in a collaborative field project of HafenCity University Hamburg, Institut Teknologi Bandung, Fraunhofer Institute for Physical Measurement Techniques (IPM), Pageo, and other partners in the Seribu National Park, Indonesia. It was mainly organized by Madam Taqiyya, Gabriella Allodia, Fickrie Muhammad, and Poerbandono. The authors would like to thank all partners and to express their special thanks to Lars Rathmann (formerly Fraunhofer IPM) for acquiring the ABS data, to the ITB team for providing the UAS batteries and to the team of Pageo for their technical support.

References

Baletti, C., Beltrame, C., Costa, E., Guerra, F., Vernier, P. , 2015. Underwater Photogrammetry and 3D Reconstruction of Mable Cargos Shipwreck. Int. Arch. Photogramm. Remote Sens. Spatial Inf. Sci., XL-5/W5, 7–13, https://doi.org/10.5194/isprsarchives-XL-5-W5-7-2015

Bleier, M., van der Lucht, J., Nüchter, A., 2019. SCOUT3D – An Underwater Laser Scanning System for Mobile Mapping. Int. Arch. Photogramm. Remote Sens. Spatial Inf. Sci., XLII-2/W18, 13–18, https://doi.org/10.5194/isprs-archives-XLII-2-W18-13-2019

Brüggemann, T., 2013. Ingenieurgeodätische Fragestellungen bei der Einmessung von Vermessungsschiffen. In: Federal Institute of Hydrology (BfG) (ed.): Neue Entwicklungen in der Gewässervermessung, Proceedings, 5/2013, Koblenz/Germany, 32-40, http://doi.bafg.de/BfG/2013/Veranst5_2013.pdf

Burns, J. H. R., Delparte, D., Gates, R. D., Takabayashi, M., 2015. Utilizing Underwater Three-Dimensional Modeling to Enhance Ecological and Biological Studies of Coral Reefs. Int. Arch. Photogramm. Remote Sens. Spatial Inf. Sci., XL-5/W5, 61–66, https://doi.org/10.5194/isprsarchives-XL-5-W5-61-2015.

Castillón, M., Palomer, A., Forest, J., Ridao, P., 2019. State of the Art of Underwater Active Optical 3D Scanners. *Sensors*, *19*(23), 5161; https://doi.org/10.3390/s19235161

Chen, Q., Yam, J. W., Chua, S. Y., Guo, N., Wang, X. (2020). Characterizing the performance impacts of target surface on underwater pulse laser ranging system. *Journal of Quantitative Spectroscopy and Radiative Transfer*, *255*. https://doi.org/10.1016/j.jqsrt.2020.107267

CloudCompare, 2022. CloudCompare wiki (V2.6 and higher). URL: https://www.cloudcompare.org/ (last accessed: 29 Mar 2026)

CloudCompare, 2024. CloudCompare Software, Version v2.13.2. LPGL version 2.0. URL: https://www.cloudcompare.org/doc/wiki/index.php/Main_Page (last accessed: 14 Nov 2025)

Guenther, G.C., 1995. Airborne Laser Hydrography – System Design and Performance Factors. *NOAA Professional Paper Series*. Springfield, VA/USA: National Technical Information Service.

Heffner, E., Walter, A.L., Scheider, A., Sternberg, H., 2025a. Laboratory-based assessment of the Underwater Laser Scanner ULi. *International Archives of the Photogrammetry, Remote Sensing and Spatial Information Sciences - ISPRS Archives*, *48*(2/W10-2025), 123–129. https://doi.org/10.5194/isprs-Archives-XLVIII-2-W10-2025-123-2025

Heffner, E., Semmelroth, C., Sternberg, H., 2025b. Untersuchung der Messeigenschaften des Unterwasser Laserscanners Uli in unterschiedlichen Temperaturbereichen als Grundlage für kombiniertes Unterwassermonitoring. In: Lienhart, W. (ed.), Ingenieurvermessung 2026, Verlag der technischen Universität Graz. DOI: 10.3217/978-3-99161-070-0-010.

Höhle, J., 1971. Zur Theorie und Praxis der Unterwasser-Photogrammetrie. In: Schriften der DGK, Reihe C, 163, Bayrische Akademie der Wissenschaften.

IHO, 2011. Manual on Hydrogaphy – Publication C-13. URL: https://iho.int/en/capacity-building-publications (last accessed: 02 Apr 2026)

IPM, 2025. Airborne Bathymetric Laser Scanner – Measuring seabed topography. Datasheet. URL: https://www.ipm.fraunhofer.de/en/bu/object-shape-detection/applications/underwater-laserscanning/bathymetry.html (last accessed: 30 Mar 2026)

IPM, 2026. Underwater LiDAR System – Optical inspection of underwater infrastructure. Datasheet. URL: https://www.ipm.fraunhofer.de/content/dam/ipm/en/PDFs/product-information/OF/AUS/Underwater-LiDAR-ULi.pdf (last accessed: 30 Mar 2026)

Kongsberg, 2022. EM 2040P MKII. Data sheet, URL: https://www.kongsberg.com/discovery/seafloor-mapping/em/EM2040P-MkII/#downloads (last accessed: 29 Mar 2026)

Lan, Y., Yang, J., Kolling, M., Dorndorf, A., Paffenholz, J.-A., 2025. Uncertainty assessment of a green-wavelength LiDAR in laboratory environments. In: Lienhart, W. (ed.), Ingenieurvermessung 2026, Verlag der technischen Universität Graz. DOI: 10.3217/978-3-99161-070-0-009

Lochhead, I. and Hedley, N., 2022. Evaluating the 3D Integrity of Underwater Structure from Motion Workflows. Photogram Rec, 37, 35-60. https://doi.org/10.1111/phor.12399

Mandlburger, G., Pfennigbauer, M., 2011. Airborne hydrographic LiDAR mapping—Potential of a new technique for capturing shallow water bodies. URL: https://www.mssanz.org.au/modsim2011/E14/mandlburger.pdf (last accessed: 21 Mar 2026)

NOAA, 2023. World Ocean Atlas 2023 – Salinity. URL: https://www.ncei.noaa.gov/access/world-ocean-atlas-2023f/ (last accessed: 19 Mar 2026)

Rebolj, D., Pučko, Z., Čuš Babič, N., Bizjak, M., Mongus, D., 2017. Point cloud quality requirements for Scan-vs-BIM based automated construction progress monitoring. Automation in Construction, Volume 84, 2017, 323-334, https://doi.org/10.1016/j.autcon.2017.09.021

SBG, 2025a. SBG Support Center – High Performance Home / Documentation & resources. URL: https://support.sbg-systems.com/sc/hp/latest/documentation-resources/quanta-micro-documentation/performance-specifications (last accessed: 30 Mar 2026)

SBG, 2025b. SBG Support Center – Qinertia documentation: Lever Arm Estimation. URL: https://support.sbg-systems.com/sc/qd/latest/reference-manual/lever-arm-estimation (last accessed: 30 Mar 2026)

Seube, N., Keyetieu, R., 2017. Multibeam Echo Sounders-IMU Automatic Boresight Calibration of Natural Surfaces. *Marine Geodesy*, *40*(2–3), 172–186. https://doi.org/10.1080/01490419.2017.1310156

Walter, A.L., Heffner, E., Scheider, A., Sternberg, H., 2025. Underwater Laser Scanning: Integration and Testing in different environments. FIG Working Week 2025, 6-10 April 2025, Brisbane, Australia. URL: https://www.fig.net/resources/proceedings/fig_proceedings/fig2025/papers/ts08g/TS08G_walter_heffner_et_al_13157.pdf (last accessed: 14 Nov 2025)

Werner, C.S., Gangelhoff, J., Frey, S., Reiterer, A., 2023. Development of a compact pulsed time of flight LiDAR platform for underwater measurements. *The International Hydrographic Review*, *29*(2), 200–207. https://doi.org/10.58440/ihr-29-2-n09